Dichroism of diamond grains by a polarization modulated near field optical setup

Ruggero Micheletto[a] and Yoichi Kawakami
Department of Electronic Science, Graduate School of Engineering, Kyoto University, Nishigyo-ku, Katsura, 615-8510 Kyoto, Japan

Claudio Manfredotti and Yiuri Garino
Department of Experimental Physics, University of Torino, Via P. Giuria, 1, 10125 Torino, Italy

Maria Allegrini
Department of Physics "E. Fermi," University of Pisa, Largo Pontecorvo 3, 56127 Pisa, Italy

(Received 20 April 2006; accepted 18 July 2006; published online 22 September 2006)

Diamond grown by chemical vapor deposition (CVD) was investigated using a polarization modulated scanning near field optical microscope. The authors found that the luminescence has spatial inhomogeneities and it is partially polarized. Confined emission shows differences in polarization angle up to 90°. The study reveals a peculiar confined dichroic behavior in CVD materials and suggests that local crystal aggregates play a role in it. © *2006 American Institute of Physics*. [DOI: 10.1063/1.2338581]

Chemical vapor deposited (CVD) diamond is characterized by exceptional mechanical and physical properties such as extremely high Young modulus, large thermal conductivity, very high radiation resistance, high transparency from UV to IR, and various other outstanding properties.[1] Diamond has been considered for numerous industrial applications as optical windows for power lasers,[2] nuclear sensors,[3] x ray,[4] and UV detectors[5] to cite a few. Unfortunately, material quality[6] is a critical factor for most of these applications, but with the recent improvement of depositing single crystal diamond films with homoepitaxy, CVD diamond has now reached a real detector grade quality.[7] Competing behavior of nearby grains that tend to expand in three dimensions induces defective regions in the intergrain domains. This results in morphological, electrical, and optical inhomogeneities of micron and submicron dimensions. Methods to investigate in high resolution these phenomena are extremely important. Defects are often related to anisotropy and strain in the crystal structure. These anysotropies can be asymmetric[8] and may induce polarization effects in the photoluminescence.[9] By using a polarization modulated scanning near field optical microscopy (PM-SNOM) setup we could study the polarization properties of photoluminescence at the submicron scale. We found regions that have distinct dichroic properties and we show their phase maps that reveal orientations that differ up to 90°; this points toward the existence of peculiar structural asymmetries and strain within the polycrystalline framework of the CVD diamond.

Emission is examined by scanning near field optical microscope fitted with a nano-apertured optical probe.[10–13] The probe-sample distance is in the order of few tens of nanometers, it is monitored and kept constant using shear force method.[14] The optical configuration is described in Fig. 1: a $\lambda=442$ nm He–Cd laser (Kimmon, Ik series, 300 mW) is used as source, light passes through a beam expander and a $\lambda/4$ plate in order to obtain a quasicircular polarization.

This signal is then filtered by a Polaroid that is mounted on a rotating motor (a modified light-chopper actuator) at a frequency of about $\omega_r=70$ Hz. Light is then guided to an objective lens (Nikon, $40\times/0.60$) that focalizes on the sample. The light emitted is collected by the near field probe, color filtered at 470 nm, and detected by a photomultiplier the (PMT). The intensity values obtained are then fed to a lock-in amplifier that is tuned with the Polaroid rotating frequency ω_r. A personal computer records simultaneously the two signals and generates two maps, the near field intensity map from the PMT, called SNOM image, and the map of the data from the lock-in, called hereafter PM-SNOM map.

The physical meaning of a SNOM map is well known;[10] it represents the intensity of the evanescent optical field in the vicinity of the sample surface. A PM-SNOM map[15–17] is instead the results of the lock-in filtering, so it is an information related to the local polarization properties of the sample.

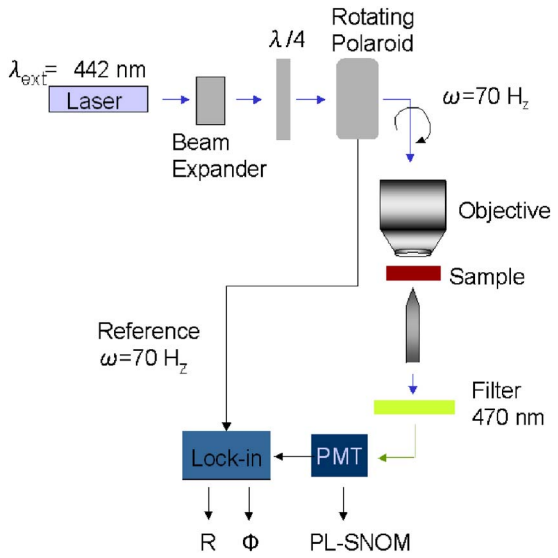

FIG. 1. (Color online) Sketch of the polarization modulated SNOM setup. Near field signal and lock-in polarization properties maps are collected simultaneously.

[a]Electronic mail: ruggero@fujita.kuee.kyoto-u.ac.jp

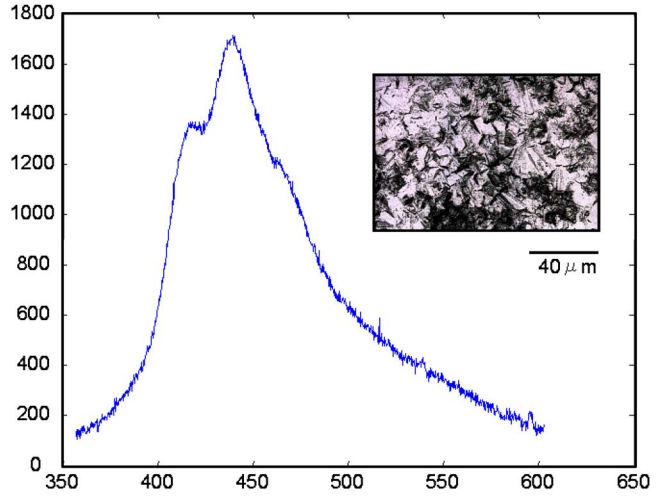

FIG. 2. (Color online) Bulk luminescence emission spectrum of our diamond sample under $\lambda=325$ nm illumination. In the inset is shown a SEM image of its surface. The thickness of the diamond is about 600 μm and its roughness is about 1 μm.

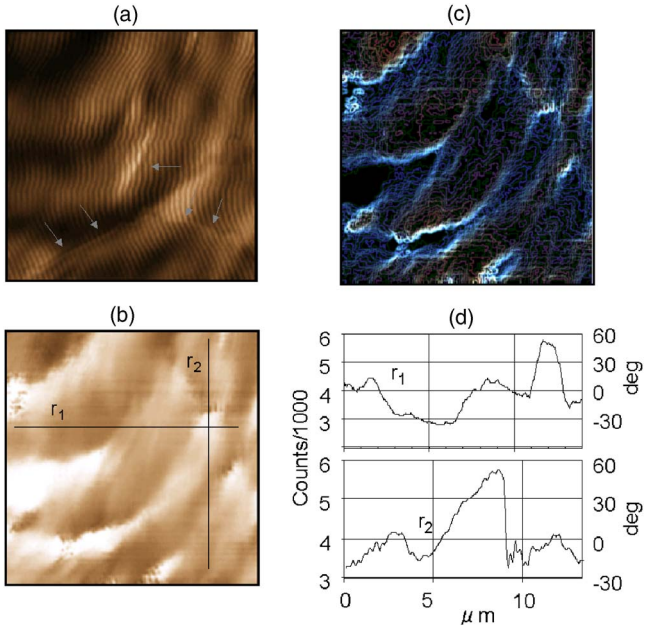

FIG. 3. (Color online) Simultaneous scans of near field photoluminescence and its polarization properties. (a) Near field PL intensity map of a 15 $\times 15$ μm^2 region. The image is not treated and oscillation due to the chopping procedure is visible. (b) Lock-in phase signal revealing pixel-to-pixel correspondence to the polarization-changing properties of the emission. (c) Map of the phase differences in (b) emphasizing the confined domains where stronger phase variation occurs. (d) Cross section along r_1 and r_2 lines. The left vertical axis corresponds to the observed signal in counts, the right one is the corresponding polarization phase shift.

If the sample does not affect the polarization of the light, the intensity at the phototube will be constant in time. Instead, where there is local dichroism, signal will be oscillating at ω_r. The amplitude of the oscillation represents how elliptic the beam is and it is measured directly at the phototube (PMT). A zero to one type of signal at PMT represents a linear polarization whereas a 0.9 to one signal represents an elliptic beam with 10% ratio between the two axes. The PM-SNOM map is then produced using the lock-in generated intensity-independent phase signal. The nanoprobe scans the sample along the *xy* plane recording a map of polarization angles, in the case of elliptic light it represents the angle of the major axis of the ellipse. The light is impinged on the opposite side of the diamond and crosses all the thickness of the sample. Polarization status will change in the bulk of the crystal and only the final polarization state will be observed by the nanoprobe. The setup essentially compares the final and initial polarization characteristics of the light. The initial status is known (linear polarization with polarization angle rotating at 70 Hz) and the probe placed in the proximity of the sample measures the final state. The sample is scanned on the *xy* plane, only the position-dependent polarization properties are relevant in these maps. Polarization changes introduced by the birefringence of the tip or other spurious phenomena will result in a mere background offset in the PM-SNOM image.

Figure 2 shows the emission spectrum of the bulk diamond crystal detected in far field and in the inset a scanning electron microscopy (SEM) image of its surface. Evident irregular crystal structures are visible; roughness, defined as the deviation from a perfectly flat surface, is about 1 μm.

Three simultaneous maps are recorded and shown in Fig. 3: the near field optic emission map (a), the polarization phase map (b), and its difference map (c). In (a) there are visible stripes caused by signal wavering due to a residual light ellipticity of about 15%. This background position-independent value is due to spurious polarization introduced by the optical probe and the bulk of the sample, which is about 600 μm thick. The other lock-in generated maps (b) and (c) concern the relevant position-dependent information. Evident domains of higher optical emission in map (a) are emphasized by arrows. The phase map represents the angular phase of the polarized optical signal in the proximity of the sample. In (c) the relative phase difference map is shown. The large circular arc patterns in (a) can be assigned to far field diffractive phenomena from the bulk of the sample. Near field related nanometer-sized structures are also visible, superimposed to the main pattern. One of those, a linear 150 nm feature, plus other even smaller filaments and other domains are indicated by arrows in (a). None of these have a corresponding counterpart in (b), demonstrating that there are no artifacts due to cross-talk and confirming that we are actually observing local polarization properties of the emission. Since the lock-in generated (b) is a map of relative angles, we also calculated its difference (c) in order to extract a direct information on the phase-changing local properties of the sample. Obvious microscopic linear boundaries are shown in this map, revealing inhomogeneous local dichroism. Even if images are contrast enhanced for visibility, the strength of this phenomenon can be calculated by treating the absolute signal values that are preserved in the actual data files and used with instrument calibration curves. The lock-in amplifier generates the signal according to its phase-voltage curve and subsequently an analog to digital (A/D) card converts this value to a unit labeled "counts" by the instrument. Lock-in response is almost linear with inclination of about 16.9°/V; 0° corresponds to 0 V. The A/D converter responds also linearly with a sensitivity, $\sigma_s=562V_l+2050$ where σ_s is in counts/V and V_l is the lock-in output in volts; with these parameters we can estimate easily the actual local dichroism effect measured on each local feature mapped. Result of this is shown in the cross section (d) along the lines r_1 and r_2 which are plotted with the corresponding phase shift values in degrees. These intriguing local polariza-

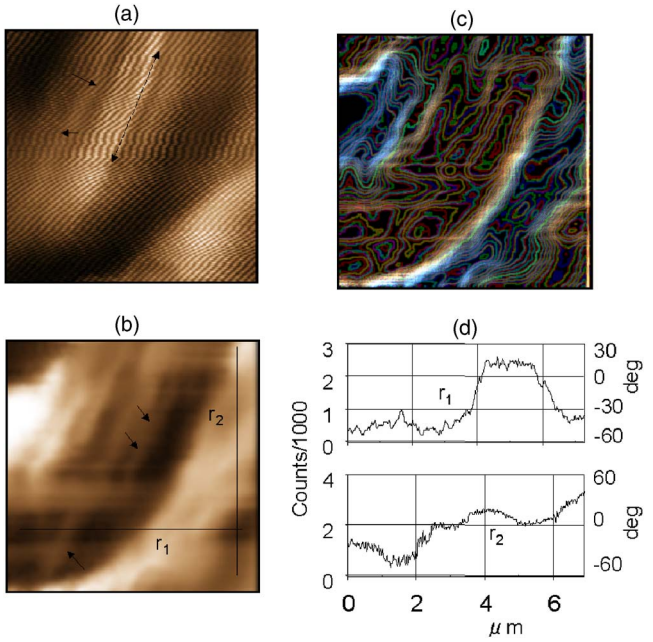

FIG. 4. (Color online) Another example of polarization-changing features within the CVD crystal structure. (a) Optical near field map. (b) Polarization modulated map. (c) Map of the phase difference emphasizing the region of higher polarization variation. (d) Cross section profiles along the lines r_1 and r_2.

tion properties of the diamond surface are presumably related to the grain orientation and spatial distribution that affect the near field coupling between optical emission and nanoprobe. Another example is Fig. 4 where in the optical SNOM image we observe an elongated superficial crystal structure, whereas in the polarization modulated image new filamentous submicron structure emerges return. We used a polarization modulated scanning near field optical microscope to probe locally the optical properties of a CVD grown diamond crystal. Its polarization-changing characteristics were recorder simultaneously and a pixel-to-pixel analysis revealed the presence of previously unseen submicron structures. This suggests that optical interaction within the crystal is not trivial and implies complex polarization effects. The molecular orientation of crystal aggregations forms geometrical anisotropy that depending on the emission polarization angle plays a of role enhancing or reducing the coupling, resulting in an increased or reduced intensity at the detector. The lock-in based method introduced here has the advantage to be very simple and straightforward and allows an immediate visualization of such polarization effects. Submicron polarization-changing structures have been recognized and quantified giving new clues to the study of CVD diamond materials that we believe will be useful for the fundamental investigation on these samples.

The authors acknowledge the Italy-Japan bilateral Project 2A2 "Surface analysis and nanocharacterization of innovative materials by scanning probe microscopy techniques" for financial support.

[1]W. A. Yarbrough and R. Messier, Science **247**, 688 (1990).
[2]A. M. Zaitsev, *Optical Properties of Diamond* (Springer, Berlin, 2001).
[3]C. Manfredotti, Diamond Relat. Mater. **14**, 531 (2005).
[4]P. J. Sellin and A. Galbiati, Appl. Phys. Lett. **87**, 93502 (2005).
[5]M. Razeghi and A. Rogalski, J. Appl. Phys. **79**, 7433 (1996).
[6]A. T. Collins, Isr. J. Chem. **38**, 121 (1998).
[7]H. Pernegger, S. Roe, P. Wheilhammer, V. Eremin, H. Frais-Keobl, E. Grismayer, H. Kagan, S. Schnetzer, R. Stone, W. Trischuk, D. Twichen, and A. Whitehead, J. Appl. Phys. **97**, 073704 (2005).
[8]O. Stier, M. Grundmann, and D. Bimberg, Phys. Rev. B **59**, 5688 (1999).
[9]R. Micheletto, J. Matsui, N. Yoshimatsu, M. Oyama, and S. Okazaki, Colloid Polym. Sci. **280**, 1067 (2002).
[10]E. Betzig, J. K. Trautman, T. D. Harris, J. S. Weiner, and R. L. Kostelak, Science **251**, 1468 (1991).
[11]T. Pangaribuan, K. Yamada, S. Jiang, H. Ohsawa, and M. Ohtsu, Jpn. J. Appl. Phys., Part 2 **31**, L1302 (1992).
[12]P. Lambelet, A. Sayah, M. Pfeffer, C. Philipona, and F. Marquis-Weible, Appl. Opt. **37**, 7289 (1998).
[13]R. Stockle, C. Fokas, V. Deckert, R. Zenobi, B. Sick, B. Hecht, and U. P. Wild, Appl. Phys. Lett. **75**, 160 (1999).
[14]W. Gohde, J. Tittel, T. Basche, C. Brauchle, U. C. Fischer, and H. Fuchs, Rev. Sci. Instrum. **68**, 2466 (1997).
[15]A. Ambrosio, M. Alderighi, M. Labardi, L. Pardi, F. Fuso, M. Allegrini, S. Nannizzi, A. Pucci, and G. Ruggeri, Nanotechnology **15**, S270 (2004).
[16]M. Labardi, N. Coppede, L. Pardi, M. Allegrini, M. Giordano, S. Patane, A. Arena, and E. Cefali, Mol. Cryst. Liq. Cryst. **398**, 33 (2003).
[17]L. Ramoino, M. Labardi, N. Maghelli, L. Pardi, M. Allegrini, and S. Patane, Rev. Sci. Instrum. **73**, 2051 (2002).